Research Article Vol. 31, No. 9 / 24 Apr 2023 / Optics Express 14037
Optics EXPRESS

Annular and unidirectional transverse scattering with high directivity based on magnetoelectric coupling

KAIHAO ZHENG,[1] WENJIA LI,[1,*] BOTIAN SUN,[1] YEHAN WANG,[1] CHUNYING GUAN,[1] JIANLONG LIU,[1] AND JINHUI SHI[1,2]

[1] *Key Laboratory of In-Fiber Integrated Optics of Ministry of Education, College of Physics and Optoelectronic Engineering, Harbin Engineering University, Harbin 150001, China*
[2] *shijinhui@hrbeu.edu.cn*
[*] *liwenjia@hrbeu.edu.cn*

Abstract: Transverse scattering is a special directional scattering perpendicular to the propagation direction, which has attracted great interest due to its potential applications from directional antennas, optical metrology to optical sensing. Here we reveal annular transverse scattering and unidirectional transverse scattering by magnetoelectric coupling of Omega particle. The annular transverse scattering can be achieved by the longitudinal dipole mode of the Omega particle. Furthermore, we demonstrate the highly asymmetric unidirectional transverse scattering by adjusting the transverse electric dipole (ED) and longitudinal magnetic dipole (MD) modes. Meanwhile, the forward scattering and backward scattering are suppressed by the interference of transverse ED and longitudinal MD modes. In particular, the lateral force exerted on the particle is accompanied by the transverse scattering. Our results provide a useful toolset for manipulating light scattered by the particle and broaden the application range of the particle with magnetoelectric coupling.

1. Introduction

Directional scattering of light by subwavelength particles, arising from the interference of optically induced modes, has attracted surging interest due to its broad application in antenna, optical sensing, optical metrology, and biomedicine [1–6]. In 1983, Kerker et al. unveiled the possibility of forward-backward giant asymmetric scattering utilizing a subwavelength particle which is widely used in Huygens metasurfaces and Mie-resonant meta devices [7–14]. Disregarding the contribution of higher-order modes, the exact reason for such forward scattering originates from the interference of induced electric dipole (ED) and magnetic dipole (MD) modes with the same amplitude and in-phase which is called the first Kerker condition [15]. Similarly, the out-phase ED and MD modes result in the backward scattering corresponding to the second Kerker condition [16,17]. It can be extended to the broader situation including perfect magnetic mirror, magnetic mirror metasurface and plasmonic-induced transparencies by coherent coupling with the quadrupole and magnetic dipole modes or toroidal and electric dipole modes, respectively [18–20]. Recently, many efforts have been devoted to manipulate the transverse scattering perpendicular to the direction of propagation, by suppressing forward and backward scattering, enriching the means of modulating the light scattering field, which is known as the transverse Kerker effect [21–31].

According to the intensity distribution of the scattered field, transverse scattering can be divided into three types: unidirectional transverse scattering [27–30], bidirectional transverse scattering [25,31] and annular transverse scattering [21,26]. The transverse Kerker effect can be achieved by carefully designing exciting sources, for example, a highly focused electromagnetic wave polarized in the azimuthal direction can induce both a longitudinal magnetic dipole and a

#485916 https://doi.org/10.1364/OE.485916
Journal © 2023 Received 18 Jan 2023; revised 11 Mar 2023; accepted 28 Mar 2023; published 13 Apr 2023

Optics EXPRESS

transverse electric dipole with equal amplitude and phase, resulting in unidirectional transverse Kerker scattering [27,28]. Besides, unidirectional transverse scattering has been achieved by manipulating the polarization states and phase shifts between two coherent plane waves illuminating at a silicon nanodisk [29]. The concept of the transverse Kerker effect has also been proposed based on dipole sources that lead to the annular and bidirectional transverse scattering [31]. Furthermore, the annular transverse scattering in subwavelength particles has been proposed when in-phase ED and MD modes with the same amplitude are out of phase with the corresponding quadrupole modes [21,26]. Recently, the V-shaped silicon nanoantenna was optimized to achieve unidirectional transverse light scattering by the interaction between dipoles and quadrupoles [30]. To date, it is a challenge to achieve transverse scattering based on the property of a simple particle structure without specific light sources and higher-order multipoles.

Compared with ordinary particles, particles with magnetoelectric coupling can expand the types of modes in particles and make the mode interference of particles more diverse, which is conducive to the realization of different types of scattering [32,33]. Taking advantage of this property, forward or backward directional scattering have been demonstrated by breaking the mirror symmetry of a single particle, spherical two-particle and metasurfaces [34–38]. Notably, the physical mechanism of transverse scattering is different from that of forward and backward directional scattering. In recent years, the investigation of the effects of magneto-dielectric materials on the optical radiation force has gained significant attention. The electric-magnetic dipolar interaction has been shown to significantly impact the force exerted on magnetodielectric particles by various types of light beams, including Bessel (vortex) beams, Fabry-Perot interferometer, and evanescent Bessel beams [39–42]. These findings have important implications for the development of novel technologies, such as particle manipulation, optical levitation, and tractor beam tweezers.

Here, we propose two schemes to achieve transverse scattering by Omega particles with magnetoelectric coupling. We theoretically give detailed analytical expressions to describe the required conditions for the annular and unidirectional transverse scattering based on magnetoelectric coupling. The phase and amplitude of the excited dipole modes can be controlled effectively by adjusting the geometric parameters to achieve different types of transverse scattering, including annular transverse scattering that eliminates both forward and backward scattering and unidirectional transverse scattering with transverse scattering asymmetry of over 30 dB. In addition, we explore the lateral optical forces generated by the interaction between light and particles. The results provide theoretical and application values in directional antennas, optical metrology, and optical sensing.

2. Theoretical model

We start with a subwavelength Omega particle with magnetoelectric coupling illuminated by a linearly polarized light as shown in Fig. 1. The Omega particle consists of a cylindrical 'electric atom' and a 'C' shaped 'magnetic atom', both of them are made of PEC and have the same radius. The geometric parameters of the Omega particle are given in Fig. 1(a). The surrounding medium is a free space. The incident plane wave is assumed to propagate along the y axis with $\mathbf{E}_{\text{in}} = \mathrm{E}_0 \mathrm{e}^{ik_0 \cdot y}\hat{\mathbf{x}}$ and $\mathbf{H}_{\text{in}} = -\mathrm{H}_0 \mathrm{e}^{ik_0 \cdot y}\hat{\mathbf{z}}$, where $k_0 = \omega/c$ is the wave number in vacuum, $\mathrm{E}_0 = \eta \mathrm{H}_0$. In the case of electrically small particles, we approximately ignore the higher-order multipoles and only consider the lowest order multipoles, usually the electric and magnetic dipoles. In the SI system of units, the electric and magnetic dipole moments induced by plane waves in the particle can be expressed as [36]

$$\boldsymbol{p} = \bar{\alpha}_{\text{ee}} \cdot \mathbf{E}_{\text{in}} + \bar{\alpha}_{\text{em}} \cdot \mathbf{H}_{\text{in}}, \tag{1}$$

$$\boldsymbol{m} = \bar{\alpha}_{\text{me}} \cdot \mathbf{E}_{\text{in}} + \bar{\alpha}_{\text{mm}} \cdot \mathbf{H}_{\text{in}}, \tag{2}$$

where $\bar{\alpha}_{\text{ee}}$, $\bar{\alpha}_{\text{em}}$, $\bar{\alpha}_{\text{me}}$ and $\bar{\alpha}_{\text{mm}}$ are the 3×3 polarizability tensors. Considering the magnetoelectric coupling in the x- and y-directions for the particle, the polarizability tensors can be written as

Optics EXPRESS

[33,43,44]

$$\bar{\alpha}_{\mathrm{ee}} = \begin{pmatrix} \alpha_{\mathrm{ee}}^{xx} & 0 & 0 \\ 0 & \alpha_{\mathrm{ee}^{yy}} & 0 \\ 0 & 0 & \alpha_{\mathrm{ee}}^{zz} \end{pmatrix}, \bar{\alpha}_{\mathrm{em}} = \begin{pmatrix} \alpha_{\mathrm{ee}}^{xx} & 0 & 0 \\ 0 & \alpha_{\mathrm{ee}^{yy}} & 0 \\ 0 & 0 & \alpha_{\mathrm{ee}}^{zz} \end{pmatrix},$$
$$\bar{\alpha}_{\mathrm{me}} = \begin{pmatrix} 0 & \alpha_{\mathrm{me}}^{xy} & 0 \\ \alpha_{\mathrm{me}}^{yx} & 0 & 0 \\ 0 & 0 & \alpha_{\mathrm{mm}}^{zz} \end{pmatrix}, \bar{\alpha}_{\mathrm{mm}} = \begin{pmatrix} \alpha_{\mathrm{mm}}^{xx} & 0 & 0 \\ 0 & \alpha_{\mathrm{mm}}^{yy} & 0 \\ 0 & 0 & \alpha_{\mathrm{mm}}^{zz} \end{pmatrix}. \tag{3}$$

When the x-polarized electric field incidents, the induced dipole moments of the Omega particle can be decomposed into the electric dipole (p_x, 0, 0) and magnetic dipole (0, m_y, m_z). Hence, the induced dipole moments can be given by

$$\begin{aligned} p_x &= \alpha_{\mathrm{ee}}^{xx} \mathrm{E}_0, \\ m_y &= \alpha_{\mathrm{me}}^{yx} \mathrm{E}_0, \\ m_z &= \alpha_{\mathrm{mm}}^{zz} \mathrm{H}_0. \end{aligned} \tag{4}$$

Based on the dipole model, the scattered electric and magnetic fields in the far field can be defined as [45]

$$\mathbf{E}_{\mathrm{sc}} = \frac{{k_0}^2}{4\pi\varepsilon_0 r} e^{ik_0 r} \left[(\hat{\mathbf{n}} \times \mathbf{p}) \times \hat{\mathbf{n}} - \frac{1}{c\mu_0} \hat{\mathbf{n}} \times \mathbf{m} \right], \tag{5}$$

$$\mathbf{H}_{\mathrm{sc}} = \frac{1}{\eta} \hat{\mathbf{n}} \times \mathbf{E}_{\mathrm{sc}}, \tag{6}$$

where ε_0 is the vacuum permittivity, μ_0 is the vacuum permeability, η is the vacuum impedance, r is the distance from a point on the scattering field to the Omega particle. $\hat{\mathbf{n}}$ is the unit vector in the direction of observation. In the spherical coordinate system, the scattered fields induced by the Omega particle can be expanded as [30,44]

$$\begin{aligned} \mathbf{E}_{\mathrm{sc}} = \frac{{k_0}^2}{4\pi\varepsilon_0 r} e^{ik_0 r} [& p_x(-\sin\varphi\hat{\varphi} + \cos\theta\cos\varphi\hat{\theta}) \\ & - \frac{1}{\eta} m_y(\cos\theta\sin\varphi\hat{\varphi} - \cos\varphi\hat{\theta}) + \frac{1}{\eta} m_z \sin\theta\hat{\varphi} \Big], \end{aligned} \tag{7}$$

where (r, θ, φ) are the spherical coordinates, θ is the elevation angle between the radial unit vector $\hat{r}$ and the forward z-axis, φ is azimuth angle corresponding to the x-axis. In consideration of the scattering cross section in the y-z plane and Eqs. (4) and (7), we derive the relation between the scattering cross section and the scalar polarizability which can be represented as

$$\begin{aligned} \sigma_{\mathrm{sca}} &= \lim_{r\to\infty} 4\pi r^2 \frac{|\mathbf{E}_{\mathrm{sc}}(\varphi = 90°, \theta)|^2}{|\mathbf{E}_{\mathrm{in}}|^2} \\ &= \frac{k^4}{4\pi{\varepsilon_0}^2 |\mathbf{E}_{\mathrm{in}}|^2} \left| \alpha_{\mathrm{ee}}^{xx} + \cos\theta \frac{\alpha_{\mathrm{me}}^{yx}}{\eta} \sin\theta \frac{\alpha_{\mathrm{mm}}^{zz}}{\eta^2} \right|^2. \end{aligned} \tag{8}$$

Equation (8) reveals that for forward and backward scattering, i.e., $\theta = 90°$ and $\theta = 270°$ it is necessary to reasonably modulate the phase and amplitude of $\alpha_{\mathrm{ee}}^{xx}$ and $\alpha_{\mathrm{mm}}^{zz}/\eta^2$ that are connected with p_x and m_z, respectively. Note that the transverse scattering ($\theta = 0°$ and $\theta = 180°$) along the z-axis is related to $\alpha_{\mathrm{ee}}^{xx}$ and $\alpha_{\mathrm{me}}^{yx}/\eta$ corresponding to the transverse electric and longitudinal magnetic

Optics EXPRESS

dipole moments. As the transverse electric dipole moment is much smaller than the magnetic dipole moment derived from the magnetoelectric coupling, the distribution of the scattered far field mainly depends on the magnetic dipole moment derived from the magnetoelectric coupling. The annular transverse scattering perpendicular to the incident direction can be achieved by suppressing the forward and backward scattering simultaneously, as shown in Fig. 1(b). Figure 1(c) shows the unidirectional transverse scattering in the negative z direction, where the phase and amplitude relationship between the scalar polarizability satisfies

$$|\eta\alpha_{\mathrm{ee}}^{xx}| = |\alpha_{\mathrm{me}}^{yx}|, \qquad \arg(\alpha_{\mathrm{ee}}^{xx}) = \arg(\alpha_{\mathrm{me}}^{yx}) + (2n+1)\pi, \tag{9}$$

where n is an integer. It means that the condition of the unidirectional transverse scattering in the negative z direction is the dipole moment p_x and m_y with the amplitude ratio and out-phase.

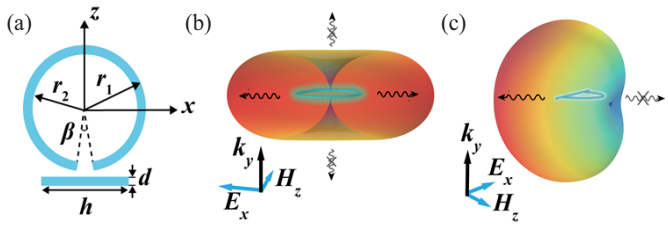

Fig. 1. (a) Geometric view of the Omega particle. Consisting of a ring with inner diameter r_1, outer diameter r_2, opening angle β, and a cylinder with height h and diameter d, where $d = r_1$-r_2. (b) Annular transverse scattering pattern for the Omega particle. (c) Unidirectional transverse scattering pattern for the Omega particle.

3. Results and discussion

In order to verify the results and predictions of our theoretical analysis, we give simulation results obtained by the commercial software COMSOL Multiphysics. The wavelength of the incident plane wave is set to $\lambda = c/f_0$ where c is the speed of light in air and f_0 is the frequency of the incident light. The geometric parameters of the C-shaped 'magnetic atom' are $r_1 = 0.085\lambda$, $r_2 = 0.076\lambda$, and $\beta = 10°$. The cylindrical 'electric atom' has a height (h) and a diameter $d = r_1$-r_2. The distance between the axis of rotation of the cylinder and the center of the ring is $D = r_1 + d$. The polarizability of the Omega particle can be regulated by adjusting the parameters [36]. The effect of β on the real and imaginary parts of the polarizability is shown in Fig. 2(a). It is clear that p_x and m_y contributions are dominant with negligible m_z contribution. The distributions of the intensity and phase of $\eta\alpha_{\mathrm{ee}}^{xx}$ and $\alpha_{\mathrm{me}}^{yx}$ as a function of β are shown in Fig. 2(b). The solid and dashed blue lines correspond to the phases of $\eta\alpha_{\mathrm{ee}}^{xx}$ and, respectively. The solid and dashed red lines with squares correspond to the magnitudes of $\eta\alpha_{\mathrm{ee}}^{xx}$ and $\alpha_{\mathrm{me}}^{yx}$, respectively. $\eta\alpha_{\mathrm{ee}}^{xx}$ is much smaller than $\alpha_{\mathrm{me}}^{yx}$ at $\beta = 10°$ which means that p_x contributes little to the scattered field. Therefore, the annular transverse scattering can be achieved by the magnetic dipole m_y that is entirely contribution to the scattered field.

Furthermore, the effect of the size parameter on the polarizability of the Omega particle is shown in Fig. 3(a). Actually, (h) is what changes with the size parameter. Evidently, p_x is minimum when the size parameter is equal to 0.75(marked by the black arrow). Figure 3(b) shows that the amplitude of reaches the minimum value as the size parameter is equal to 0.75 where the contributions of the dipole modes to the scattered field come almost entirely from the magnetic dipole. The inset of Fig. 3(b) is the ratio of the magnitudes of to $\eta\alpha_{\mathrm{ee}}^{xx}$ under different size parameters. When the size parameter is 0.75, the ratio of the magnitudes of them reaches the maximum, at which point the annular transverse scattering can be obtained [see Figs. 3(c) and

Optics EXPRESS

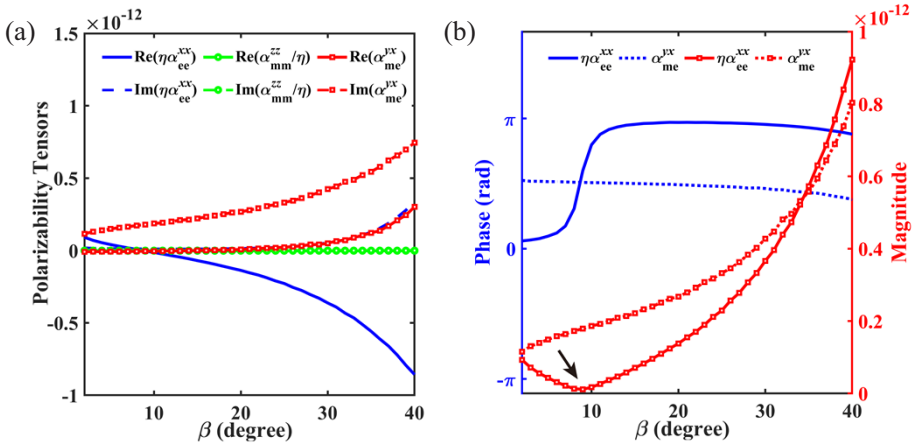

Fig. 2. (a) Dependences of real and imaginary parts of $\eta\alpha_{ee}^{xx}$, and α_{mm}^{zz}/η on opening angles of the ring (β). (b) Changes in phase and intensity of $\eta\alpha_{ee}^{xx}$ and α_{me}^{yx} of (β) from 2° to 40°.

3(d)]. In order to present the directivity of annular transverse scattering, we define the directivity by comparing the minimum of the intensity in the transverse direction with the maximum of the intensity in the forward and backward directions

$$\text{Directionality}_{\text{annular}} = 10\log_{10}\left(\frac{|E_t^{\min}|^2}{|E_{fb}^{\max}|^2}\right) \quad \text{(dB)} \tag{10}$$

where $E_t^{\min}$ is the minimum value of the intensity of scattered electric field in the transverse direction of x-z plane. $E_{fb}^{\max}$ is the maximum value of the intensity of scattering electric field in the forward and backward directions. According to Fig. 3(d), the directivity of annular transverse scattering is over 23 dB. It shows the high directivity of annular transverse scattering by great inhibition of forward and backward scattering, relative to Refs. [21] and [26].

Based on the annular transverse scattering, we proceed to discuss unidirectional transverse scattering where the induced electric and magnetic dipole modes should satisfy the condition in Eq. (9). The frequency of the incident light is 1.274 GHz. The geometric parameters of the Omega particle are chosen as $r_1 = 0.132\lambda$, $r_2 = 0.123\lambda$, $\beta = 185°$and the distance between the axis of rotation of the cylinder and the center of the ring is set to (D). The effect of the size parameter ($2r_1/h$) on the scalar polarizability of the Omega particle is shown in Fig. 4. Compared to $\eta\alpha_{ee}^{xx}$ and, the effect of α_{mm}^{zz}/η on the scattered far field can be approximately ignored. Compared with the original geometric parameters, the magnitude and phase of $\eta\alpha_{ee}^{xx}$ and α_{me}^{yx} have a larger variation range. Moreover, when size parameter is close to 1.5, they are not only equal in amplitude, but also have a phase difference($\Delta\varphi$) close to 180° as shown in Figs. 4(a) and 4(b). Hence, the unidirectional transverse scattering condition as Eq. (9) can be satisfied by adjusting the geometric parameters of the designed Omega particle.

Next, we explore the changes in the polarizability caused by the different frequencies of the incident light (f_0) when the size parameter is 1.5. Figure 5(a) presents the magnitude and phase of electric and magnetoelectric polarizabilities of the nanoparticle as a function of the frequency of the incidence (f_0). As the frequency increased to 1.274 GHz, not only did the phase difference between them reaches 180° (marked by blue dotted circles), but also the amplitude was approximately at same (marked by red dotted circles), meeting the requirements of Eq. (9). The normalized scattering cross section in Fig. 5(b) is equal to zero at this point, which is satisfied the transverse Kerker condition. The corresponding scattering patterns are shown in Figs. 5(d) and

Optics EXPRESS

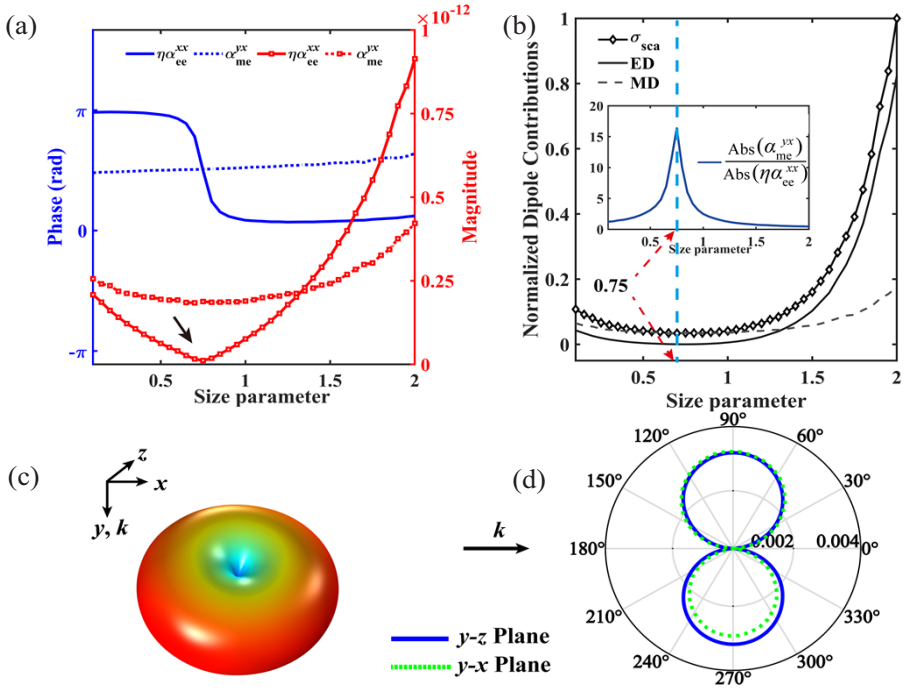

Fig. 3. (a) Changes in phase and intensity of $\eta\alpha_{ee}^{xx}$ and α_{me}^{yx} of the size parameter $(2r_1/h)$ from 0.1 to 2 where $r_1 = 0.085\lambda$, $r_2 = 0.076\lambda$, $\beta = 10°$ and $d = r_1 - r_2$. (b) Normalized contributions of electric and magnetic dipole modes to the scattering cross section, respectively. Inset: the ratio of the magnitudes of and under different size parameters. The blue dashed line corresponds to = 0.75. (c),(d) Two- and three-dimensional scattering patterns at $\lambda = 0.236m$ with $2r_1/h$= 0.75.

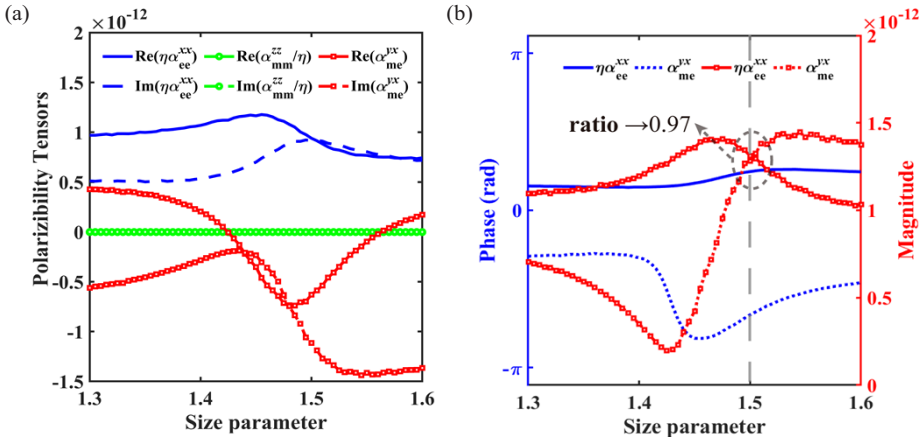

Fig. 4. (a) Real and imaginary parts of $\eta\alpha_{ee}^{xx}$, and α_{mm}^{zz}/η at different size parameter $(2r_1/h)$. (b) Changes in phase and intensity of $\eta\alpha_{ee}^{xx}$ and α_{me}^{yx} of the size parameter $(2r_1/h)$ from 1.3 to 1.6. The frequency of the incident light is 1.274 GHz. $r_1 = 0.132\lambda$, $r_2 = 0.123\lambda$, $\beta = 185°$ and $d = r_1 - r_2$.

Optics EXPRESS

5(e). Hence, the unidirectional transverse scattering in the -z axis direction can be realized, which is confirm our claim. We also define the directionality of unidirectional transverse scattering as

$$\text{Directionality} = 10\log_{10}\left(\frac{|E_{-z}|^2}{|E_{+z}|^2}\right) \quad \text{(dB)} \tag{11}$$

where $E_{\pm z}$ denote the electric field in the positive and negative z directions. Figure 5(c) shows the directionality of unidirectional transverse scattering in the -z direction at the size parameter equal to 1.5. The directivity is the highest at 1.274 GHz, exceeding 30 dB, which is a significant improvement compared with the previous work [27].

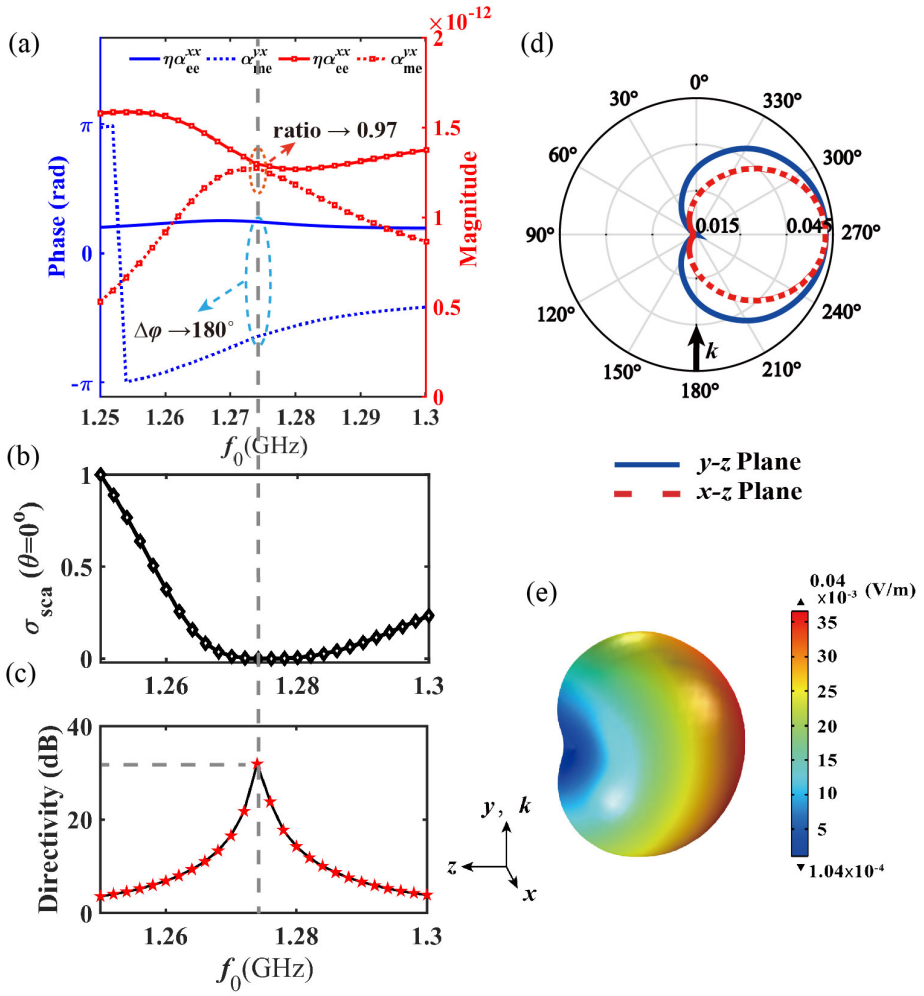

Fig. 5. (a) Changes in phase and intensity of $\eta\alpha_{ee}^{xx}$ and α_{me}^{yx} of the frequency from 1.25 to 1.3 GHz. (b) Dependences of normalized scattering cross section at $\theta = 0°$ on frequency. (c) Dependences of the radiation directivities on frequency. The maximum value is over 30 dB. (d),(e) Two- and three-dimensional scattering patterns at $f_0 = 1.274$ GHz with $2r_1/h$= 1.5.

We investigate the variation of polarizability caused by different separation distance (D) when the size parameter ($2r_1/h$) are 0.75 and 1.5, respectively. The geometric parameters of the Omega

Optics EXPRESS

particle for the annular transverse scattering are chosen as $r_1 = 0.085\lambda$, $r_2 = 0.076\lambda$, and $\beta = 10°$. As shown in Fig. 6(a), α_{me}^{yx} is much larger than $\eta\alpha_{ee}^{xx}$,which ensures that the annular transverse scattering we achieve has a strong suppression effect on the forward and backward scattering. It is clear that the ratio of α_{me}^{yx} and reaches the maximum at $D = 24$ mm. Figure 6(a) shows the dependences of real and imaginary parts of $\eta\alpha_{ee}^{xx}$ and α_{me}^{yx} on separation distance (D) for the unidirectional transverse scattering. The geometric parameters of the Omega particle for the unidirectional transverse scattering are chosen as $r_1 = 0.132\lambda$, $r_2 = 0.123\lambda$ and $\beta = 185°$. It can be seen that the condition of unidirectional transverse scattering (Eq. (9)) can be achieved at $D = 1$ mm. In general, the separation distance (D) influences the polarizability of Omega particles similar to the effect of the ring opening angle (β) and the size parameters ($2r_1/h$).

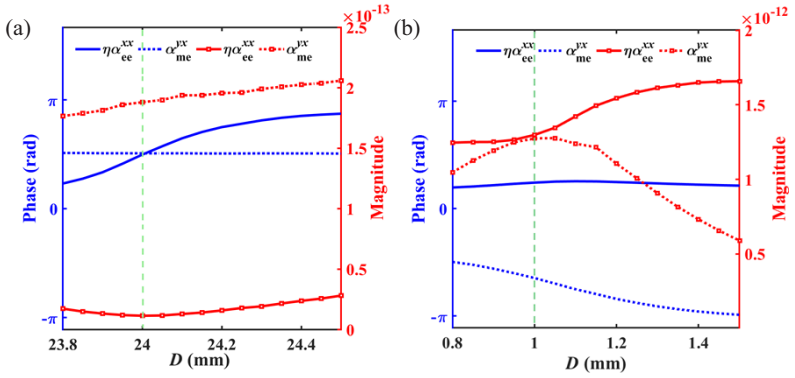

Fig. 6. Dependences of real and imaginary parts of $\eta\alpha_{ee}^{xx}$ and α_{me}^{yx} on separation distance (D) for the annular and unidirectional transverse scattering. (a) Annular transverse scattering at $2r_1/h$= 0.75 when $f_0 = 1.27$ GHz. (b) unidirectional transverse scattering at $2r_1/h = 1.5$ when $f_0 = 1.274$ GHz.

4. Lateral optical force

Since the Omega particles exhibit significant unidirectional transverse scattering phenomena, it is interesting to explore the effects of unidirectional transverse scattering on the optical scattering forces acting on the particles. The time-averaged optical force acting on a particle irradiated by an arbitrary incident light field is usually given by the surface integral of the Maxwell stress tensor

$$\langle \mathbf{F} \rangle = \oint_S \hat{n} \cdot \langle \bar{\mathbf{T}} \rangle \mathrm{d}\sigma, \tag{12}$$

where the time-averaged Maxwell stress tensor can be expressed as

$$\langle \bar{\mathbf{T}} \rangle = \frac{1}{2} Re \left[\varepsilon \mathbf{E}\mathbf{E}^* + \mu \mathbf{H}\mathbf{H}^* - \frac{1}{2}(\varepsilon \mathbf{E} \cdot \mathbf{E}^* + \mu \mathbf{H} \cdot \mathbf{H}^*)\bar{\mathbf{I}} \right], \tag{13}$$

where $\mathbf{E}$ and $\mathbf{H}$ are the total fields. ε and μ are the permittivity and permeability of the surrounding medium, respectively. is the unit tensor. Multipole expansion of optical force up to electric dipole and magnetic dipole can be written as [46–49]

$$\langle \mathbf{F} \rangle = \frac{1}{2} Re \left[(\nabla \mathbf{E}_{in}^*) \cdot \mathbf{p} + (\nabla \mathbf{H}_{in}^*) \cdot \mathbf{m} - \frac{ck_0^4}{6\pi} (\mathbf{p} \times \mathbf{m}^*) \right]. \tag{14}$$

Substitute Eq. (4) into Eq. (14), and considering incident plane wave with $\mathbf{E}_{in} = \mathrm{E}_0 e^{ik_0 \cdot y} \hat{\mathbf{x}}$, we obtain

$$\langle \mathbf{F}_x \rangle = 0, \tag{15}$$

Optics EXPRESS

$$\langle \mathbf{F}_y \rangle = \mathbf{e}_y \left\{ \frac{k_0}{2} \mathrm{H}_0^2 \mathrm{Im}(\eta^2 \alpha_{\mathrm{ee}}^{xx} + \alpha_{\mathrm{mm}}^{zz}) - \frac{ck_0^4}{12\pi} \mathrm{H}_0^2 (\eta \alpha_{\mathrm{ee}}^{xx} \alpha_{\mathrm{mm}}^{zz\,*}) \right\}, \tag{16}$$

$$\langle \mathbf{F}_z \rangle = -\mathbf{e}_z \frac{ck_0^4}{12\pi} \mathrm{H}_0^2 (\eta^2 \alpha_{\mathrm{ee}}^{xx} \alpha_{\mathrm{me}}^{yx\,*}). \tag{17}$$

Equation (17) shows that the lateral optical force on the Omega particle has a strong correlation with the magnetoelectric coupling term $\alpha_{\mathrm{me}}^{yx*}$. To prove the effectiveness of this discovery, the Maxwell pressure tensor method is used to directly calculate the optical force acting on the Omega particle, as shown in Fig. 7(a). It is clear that F_z and F_y are of comparable magnitude, while F_x is close to zero compared to both. Similar results can be seen in Fig. 7(b), which is calculated by the dipole expansion method shown in Eqs. (15)-(17). The results calculated by these two methods are consistent with each other.

Additionally, we consider a PEC sphere of radius $r_1 = 0.132\lambda$ placed in air with complete symmetry, and calculate its optical force under the same incident light using the Maxwell pressure tensor method, as shown in Fig. 7(c). We note that F_y is still on the same order of magnitude compared with the optical force on the Omega particle [see Figs. 7(a)–7(b)], but the lateral optical force F_z is almost non-existent. It can be seen that the magnetoelectric coupling characteristics play a crucial role in the generation of lateral optical force on the particle, which is substantially in accordance with our theoretical expectation. In recent years, optical nanoheating in optical frequencies has received increasing interest due to its possibilities in biomedical, clinical applications and optothermal manipulation [50,51]. Although we only consider the particle made of PEC in this paper, it is believed that the combination of thermal and optical forces is beneficial to manipulate particles [50].

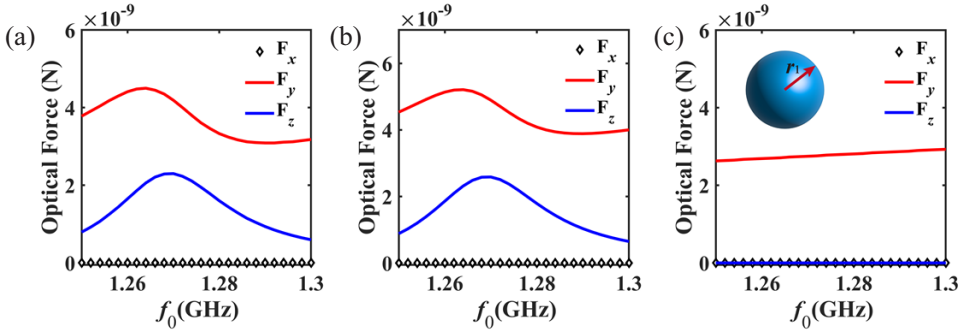

Fig. 7. (a) The components of the optical force acting on the Omega particle in the x, y, and z directions directly calculated by the Maxwell pressure tensor method, respectively. (b) The components of the optical force acting on the Omega particle in the x, y, and z directions calculated by the dipole expansion method, respectively. (c) The components of the optical force acting on an isotropic PEC sphere of radius r_1 in the x, y, and z directions with the same incident light.

5. Conclusion

To sum up, our work demonstrated that annular transverse scattering and unidirectional transverse scattering with high directionality can be achieved by the Omega particle with magnetoelectric coupling. We gave detailed analytical expressions to describe the relationship between transverse scattering and the scalar polarizability of the Omega particle. The annular transverse scattering can be achieved by tuning the geometric parameters of the Omega particle, because the longitudinal magnetic dipole response is much larger than the transverse electric dipole response. In addition,

Optics EXPRESS

the unidirectional transverse scattering with asymmetry over 30 dB can be generated by utilizing the magnetoelectric coupling property of the Omega particle. In particular, we found that the particle is subjected to an obvious lateral optical force when the unidirectional transverse scattering is present. The magnetoelectric coupling of the Omega particle plays a significant role in the enhancement of the lateral optical force. Our results pave a novel path for directional antennas, optical metrology, and efficient optical sensing.

Funding. Natural Science Foundation of Heilongjiang Province (LH2021A008); National Natural Science Foundation of China (12074087, 12204126, 62175049); 111 Project of Harbin Engineering University (B13015); Fundamental Research Funds for the Central Universities (3072022TS2501, 3072022TS2505, 3072022TS2509, 3072022CFJ2506).

Disclosures. The authors declare no conflicts of interest.

Data availability. Data underlying the results presented in this paper are not publicly available at this time but may be obtained from the authors upon reasonable request.

References

1. C. F. Bohren and D. R. Huffman, *Absorption and Scattering of Light by Small Particles* (Wiley, 1983).
2. S. Kruk and Y. Kivshar, "Functional Meta-Optics and Nanophotonics Governed by Mie Resonances," ACS Photonics **4**(11), 2638–2649 (2017).
3. D. Vercruysse, P. Neutens, L. Lagae, N. Verellen, and P. Van Dorpe, "Single Asymmetric Plasmonic Antenna as a Directional Coupler to a Dielectric Waveguide," ACS Photonics **4**(6), 1398–1402 (2017).
4. T. Shegai, P. Johansson, C. Langhammer, and M. Käll, "Directional Scattering and Hydrogen Sensing by Bimetallic Pd–Au Nanoantennas," Nano Lett. **12**(5), 2464–2469 (2012).
5. A. Bag, M. Neugebauer, U. Mick, S. Christiansen, S. A. Schulz, and P. Banzer, "Towards fully integrated photonic displacement sensors," Nat. Commun. **11**(1), 2915 (2020).
6. P. Eugui, A. Lichtenegger, M. Augustin, D. J. Harper, M. Muck, T. Roetzer, A. Wartak, T. Konegger, G. Widhalm, C. K. Hitzenberger, A. Woehrer, and B. Baumann, "Beyond backscattering: optical neuroimaging by BRAD," Biomed. Opt. Express **9**(6), 2476–2494 (2018).
7. M. Kerker, D.-S. Wang, and C. L. Giles, "Electromagnetic scattering by magnetic spheres," J. Opt. Soc. Am. **73**(6), 765 (1983).
8. M. Decker, I. Staude, M. Falkner, J. Dominguez, D. N. Neshev, I. Brener, T. Pertsch, and Y. S. Kivshar, "High-Efficiency Dielectric Huygens' Surfaces," Adv. Opt. Mater. **3**(6), 813–820 (2015).
9. I. Staude, T. Pertsch, and Y. S. Kivshar, "All-Dielectric Resonant Meta-Optics Lightens up," ACS Photonics **6**(4), 802–814 (2019).
10. W. Chen, Y. Chen, and W. Liu, "Multipolar Conversion Induced Subwavelength High–Q Kerker Supermodes with Unidirectional Radiations," Laser Photonics Rev. **13**(9), 1900067 (2019).
11. J. Olmos-Trigo, C. Sanz-Fernández, D. R. Abujetas, J. Lasa-Alonso, N. de Sousa, A. García-Etxarri, J. A. Sánchez-Gil, G. Molina-Terriza, and J. J. Sáenz, "Kerker Conditions upon Lossless, Absorption, and Optical Gain Regimes," Phys. Rev. Lett. **125**(7), 073205 (2020).
12. H. Wang, P. Liu, Y. Ke, Y. Su, L. Zhang, N. Xu, S. Deng, and H. Chen, "Janus Magneto–Electric Nanosphere Dimers Exhibiting Unidirectional Visible Light Scattering and Strong Electromagnetic Field Enhancement," ACS Nano **9**(1), 436–448 (2015).
13. L. Wei, N. Bhattacharya, and H. P. Urbach, "Adding a spin to Kerker's condition: angular tuning of directional scattering with designed excitation," Opt. Lett. **42**(9), 1776–1779 (2017).
14. V. E. Babicheva and A. B. Evlyukhin, "Resonant lattice Kerker effect in metasurfaces with electric and magnetic optical responses," Laser Photonics Rev. **11**(6), 1700132 (2017).
15. X. M. Zhang, Q. Zhang, S. J. Zeng, Z. Z. Liu, and J.-J. Xiao, "Dual-band unidirectional forward scattering with all-dielectric hollow nanodisk in the visible," Opt. Lett. **43**(6), 1275 (2018).
16. A. Alu and N. Engheta, "How does zero forward-scattering in magnetodielectric nanoparticles comply with the optical theorem?" J. Nanophotonics **4**(1), 041590 (2010).
17. W. Liu, A. E. Miroshnichenko, D. N. Neshev, and Y. S. Kivshar, "Broadband Unidirectional Scattering by Magneto-Electric Core–Shell Nanoparticles," ACS Nano **6**(6), 5489–5497 (2012).
18. Y. Yu, Y.-Q. Li, R. Salas-Montiel, and D.-Y. Qiao, "Perfect magnetic mirror based on magnetic dipole scattering in all-dielectric resonators," J. Appl. Phys. **131**(15), 153101 (2022).
19. A. K. González-Alcalde, M. A. G. Mandujano, R. Salas-Montiel, L. O. Le Cunff, G. Lerondel, and E. R. Méndez, "Magnetic mirror metasurface based on the in-phase excitation of magnetic dipole and electric quadrupole resonances," J. Appl. Phys. **125**(24), 243103 (2019).
20. F. López-Rayón, M. L. Arroyo Carrasco, R. I. Rodríguez-Beltrán, R. Salas-Montiel, and R. Téllez-Limón, "Plasmonic-Induced Transparencies in an Integrated Metaphotonic System," Nanomaterials **12**(10), 1701 (2022).
21. X. Zhang and A. L. Bradley, "Wide-angle invisible dielectric metasurface driven by transverse Kerker scattering," Phys. Rev. B **103**(19), 195419 (2021).

Optics EXPRESS

22. D. Vercruysse, Y. Sonnefraud, N. Verellen, F. B. Fuchs, G. Di Martino, L. Lagae, V. V. Moshchalkov, S. A. Maier, and P. Van Dorpe, "Unidirectional Side Scattering of Light by a Single-Element Nanoantenna," Nano Lett. **13**(8), 3843–3849 (2013).
23. G. Lu, Y. Wang, R. Y. Chou, H. Shen, Y. He, Y. Cheng, and Q. Gong, "Directional side scattering of light by a single plasmonic trimer: Directional side scattering of light by a single plasmonic trimer," Laser Photonics Rev. **9**(5), 530–537 (2015).
24. Z. Xi, L. Wei, A. J. L. Adam, H. P. Urbach, and L. Du, "Accurate Feeding of Nanoantenna by Singular Optics for Nanoscale Translational and Rotational Displacement Sensing," Phys. Rev. Lett. **117**(11), 113903 (2016).
25. J. Y. Lee, A. E. Miroshnichenko, and R.-K. Lee, "Simultaneously nearly zero forward and nearly zero backward scattering objects," Opt. Express **26**(23), 30393 (2018).
26. H. K. Shamkhi, K. V. Baryshnikova, A. Sayanskiy, P. Kapitanova, P. D. Terekhov, P. Belov, A. Karabchevsky, A. B. Evlyukhin, Y. Kivshar, and A. S. Shalin, "Transverse Scattering and Generalized Kerker Effects in All-Dielectric Mie-Resonant Metaoptics," Phys. Rev. Lett. **122**(19), 193905 (2019).
27. S. Nechayev, J. S. Eismann, M. Neugebauer, P. Woźniak, A. Bag, G. Leuchs, and P. Banzer, "Huygens' dipole for polarization-controlled nanoscale light routing," Phys. Rev. A **99**(4), 041801 (2019).
28. A. Bag, M. Neugebauer, P. Woźniak, G. Leuchs, and P. Banzer, "Transverse Kerker Scattering for Angstrom Localization of Nanoparticles," Phys. Rev. Lett. **121**(19), 193902 (2018).
29. H. Yu, H. Zhu, J. Li, Z. Cao, and H. Chen, "Broadband Active Control of Transverse Scattering from All-Dielectric Nanoparticle," Crystals **11**(8), 920 (2021).
30. Y. Yu, J. Liu, Y. Yu, D. Qiao, Y. Li, and R. Salas-Montiel, "Broadband unidirectional transverse light scattering in a V-shaped silicon nanoantenna," Opt. Express **30**(5), 7918 (2022).
31. F. Qin, Z. Zhang, K. Zheng, Y. Xu, S. Fu, Y. Wang, and Y. Qin, "Transverse Kerker Effect for Dipole Sources," Phys. Rev. Lett. **128**(19), 193901 (2022).
32. D. V. Zhirihin, S. V. Li, D. Y. Sokolov, A. P. Slobozhanyuk, M. A. Gorlach, and A. B. Khanikaev, "Photonic spin Hall effect mediated by bianisotropy," Opt. Lett. **44**(7), 1694 (2019).
33. W. Li, J. Liu, Y. Gao, K. Zhou, and S. Liu, "Enhanced spin Hall effect of light scattering on a meta-atom with bianisotropy," Phys. Rev. A **102**(6), 063527 (2020).
34. T. Feng, S. Yang, N. Lai, W. Chen, D. Pan, W. Zhang, A. A. Potapov, Z. Liang, and Y. Xu, "Manipulating light scattering by nanoparticles with magnetoelectric coupling," Phys. Rev. B **102**(20), 205428 (2020).
35. S. Sun, D. Wang, Z. Feng, and W. Tan, "Highly efficient unidirectional forward scattering induced by resonant interference in a metal–dielectric heterodimer," Nanoscale **12**(43), 22289–22297 (2020).
36. R. Alaee, M. Albooyeh, M. Yazdi, N. Komjani, C. Simovski, F. Lederer, and C. Rockstuhl, "Magnetoelectric coupling in nonidentical plasmonic nanoparticles: Theory and applications," Phys. Rev. B **91**(11), 115119 (2015).
37. R. Alaee, M. Albooyeh, A. Rahimzadegan, M. S. Mirmoosa, Y. S. Kivshar, and C. Rockstuhl, "All-dielectric reciprocal bianisotropic nanoparticles," Phys. Rev. B **92**(24), 245130 (2015).
38. M. Li, Y. Hu, Q. Chen, H. Chen, and Z. Wang, "Bianisotropic origami metasurfaces for mechanically controlled asymmetric radiation," New J. Phys. **23**(8), 085002 (2021).
39. F. G. Mitri, R. X. Li, R. P. Yang, L. X. Guo, and C. Y. Ding, "Optical pulling force on a magneto-dielectric Rayleigh sphere in Bessel tractor polarized beams," J. Quant. Spectrosc. Radiat. Transfer **184**, 360–381 (2016).
40. T. Yao, S. Pu, J. Rao, and J. Zhang, "Investigation of optical force on magnetic nanoparticles with magnetic-fluid-filled Fabry-Perot interferometer," Sci. Rep. **8**(1), 12352 (2018).
41. M. Nieto-Vesperinas, J. J. Sáenz, R. Gómez-Medina, and L. Chantada, "Optical forces on small magneto-dielectric particle," Opt. Express **18**(11), 11428 (2010).
42. J. M. Auñón and M. Nieto-Vesperinas, "Optical forces from evanescent Bessel beams, multiple reflections, and Kerker conditions in magnetodielectric spheres and cylinders," J. Opt. Soc. Am. A **31**(9), 1984 (2014).
43. R. Alaee, R. Filter, D. Lehr, F. Lederer, and C. Rockstuhl, "A generalized Kerker condition for highly directive nanoantennas," Opt. Lett. **40**(11), 2645 (2015).
44. V. S. Asadchy, I. A. Faniayeu, Y. Ra'di, and S. A. Tretyakov, "Determining polarizability tensors for an arbitrary small electromagnetic scatterer," Photonics Nanostruct. Fundam. Appl. **12**(4), 298–304 (2014).
45. J. D. Jackson, *Classical Electrodynamics*, 3rd ed (Wiley, 2001).
46. J. Chen, J. Ng, Z. Lin, and C. T. Chan, "Optical pulling force," Nat. Photonics **5**(9), 531–534 (2011).
47. S. B. Wang and C. T. Chan, "Lateral optical force on chiral particles near a surface," Nat. Commun. **5**(1), 3307 (2014).
48. H. Chen, H. Zheng, W. Lu, S. Liu, J. Ng, and Z. Lin, "Lateral Optical Force due to the Breaking of Electric-Magnetic Symmetry," Phys. Rev. Lett. **125**(7), 073901 (2020).
49. P. C. Chaumet and A. Rahmani, "Electromagnetic force and torque on magnetic and negative-index scatterers," Opt. Express **17**(4), 2224 (2009).
50. D. G. Kotsifaki and S. Nic Chormaic, "The role of temperature-induced effects generated by plasmonic nanostructures on particle delivery and manipulation: a review," Nanophotonics **11**(10), 2199–2218 (2022).
51. Y. Li, X. Yang, Y. Yang, B. Wang, X. Li, and R. Salas-Montiel, "Optical nanoheating of resonant silicon nanoparticles," Opt. Express **27**(21), 30971 (2019).